Frontiers of Materials Science

Electronic Supplementary Material

Facet–doping coupling governs ferrocene monolayer redox on silicon surfaces

Xiaojie Zhong, Xiaoxue Song, Weiqiang Zhou, Qian Yang, Shun Li, Jianming Zhang, Yuqiao Zhang (✉), and Long Zhang (✉)

Institute of Quantum and Sustainable Technology (IQST), School of Chemistry and Chemical Engineering, Jiangsu University, Zhenjiang 212013, China

E-mails: yuqiaozhang@ujs.edu.cn (Y.Z.), longzhang@ujs.edu.cn (L.Z.)

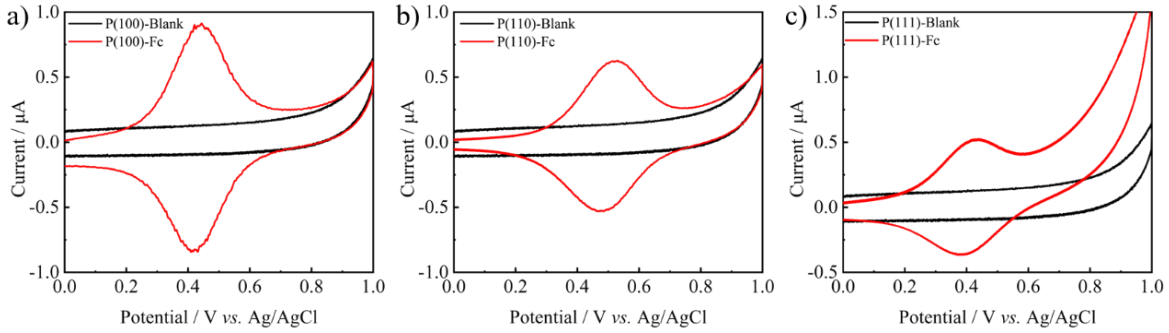

Fig. S1 Cyclic voltammograms of p-type **(a)** Si(100), **(b)** Si(110), and **(c)** Si(111) electrodes before (blank) and after Fc functionalization in 0.1 mol·L^{-1} Bu_4NPF_6/MeCN. The appearance of a Fc/Fc$^+$ redox couple after modification confirms successful formation of a surface-bound Fc layer on p-type Si.

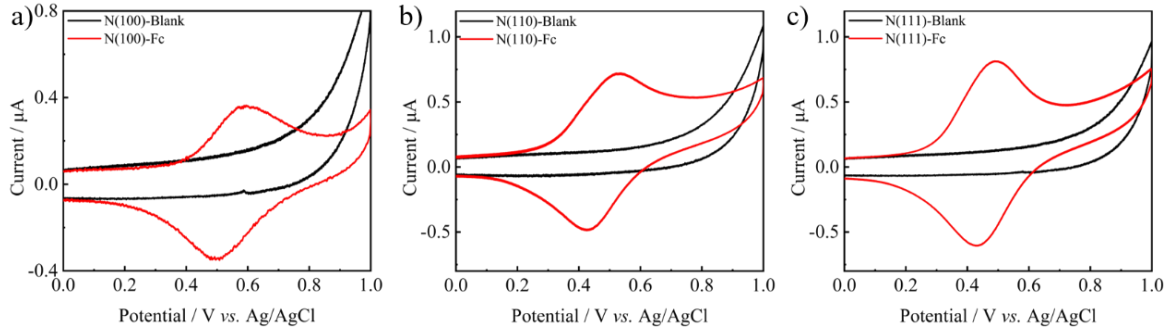

Fig. S2 Cyclic voltammograms of n-type **(a)** Si(100), **(b)** Si(110), and **(c)** Si(111) electrodes before (blank) and after Fc functionalization in 0.1 mol·L^{-1} Bu_4NPF_6/MeCN. The Fc/Fc$^+$ redox features observed only on modified electrodes indicate successful Fc grafting on n-type Si across all orientations.

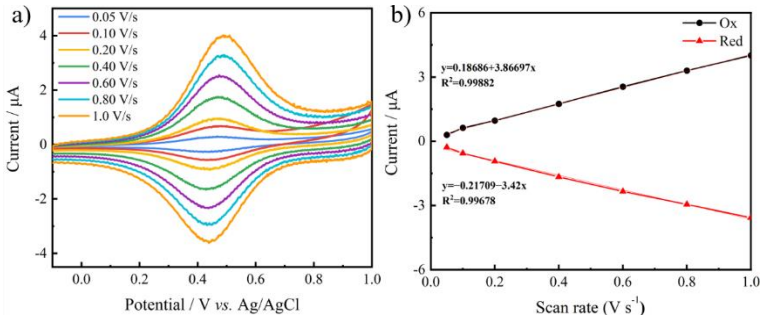

Fig. S3 Scan-rate dependence of the Fc/Fc$^+$ response on a representative Fc-modified p-type Si electrode: **(a)** CV curves recorded at different scan rates; **(b)** corresponding peak current versus scan rate plots for oxidation and reduction. The linear relationship between peak current and scan rate is consistent with a surface-confined redox process.

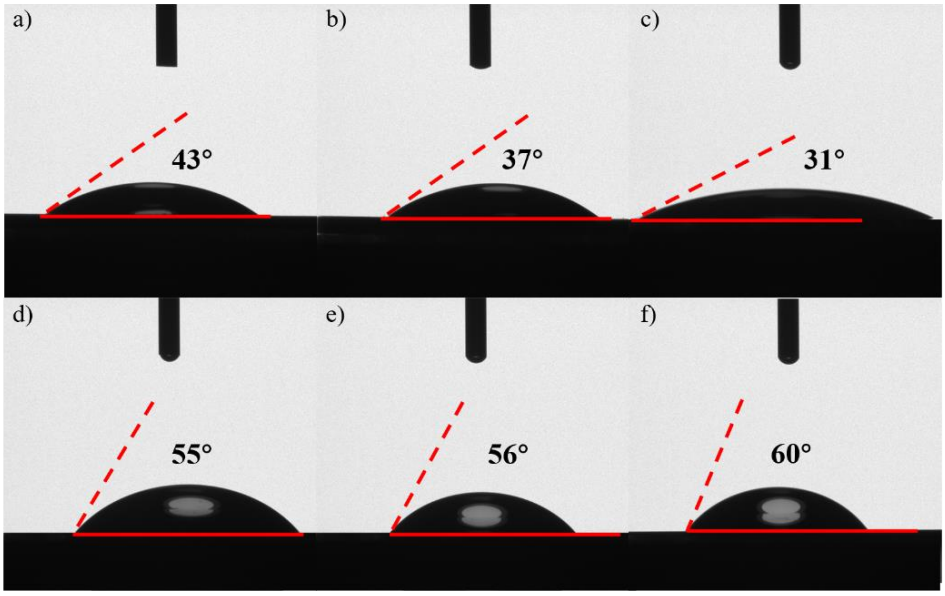

Fig. S4 Static water contact-angle measurements on n-type silicon facets before and after Fc grafting: **(a)(b)(c)** blank p-Si(100), p-Si(110), and p-Si(111) surfaces show contact angles of 43°, 37°, and 31°, respectively; **(d)(e)(f)** after Fc grafting, the contact angles increase to 55° (n-Si(100)), 56° (n-Si(110)), and 60° (n-Si(111)), respectively, consistent with the formation of an organic overlayer and reduced facet-dependent wettability.

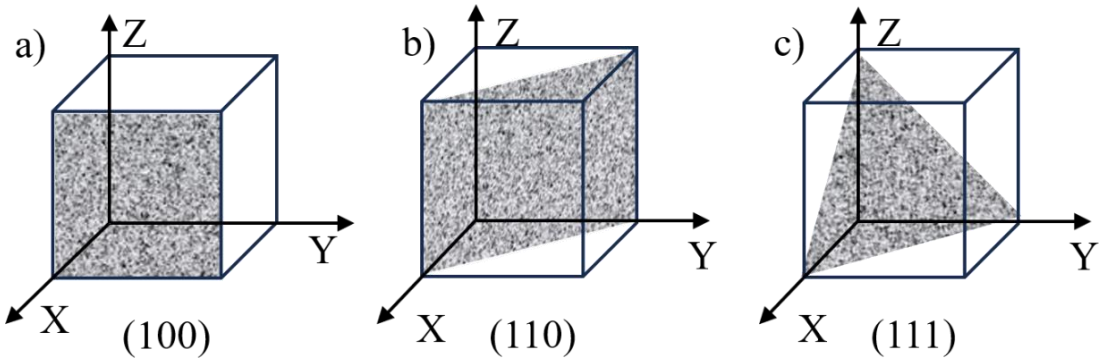

Fig. S5 Schematic representation of the low-index silicon surfaces investigated in this study: **(a)** Si(100); **(b)** Si(110); **(c)** Si(111). The shaded plane indicates the exposed facet corresponding to each crystal orientation.

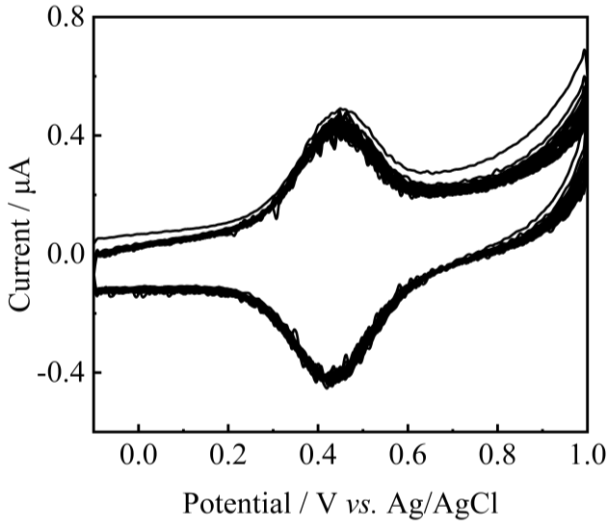

Fig. S6 Cycling stability of the P(100)-Fc modified silicon electrode. Evolution of the ferrocene surface coverage (Γ), calculated from the background-subtracted anodic charge, shows negligible change in Γ after cycling during 25 consecutive cyclic voltammetry scans.

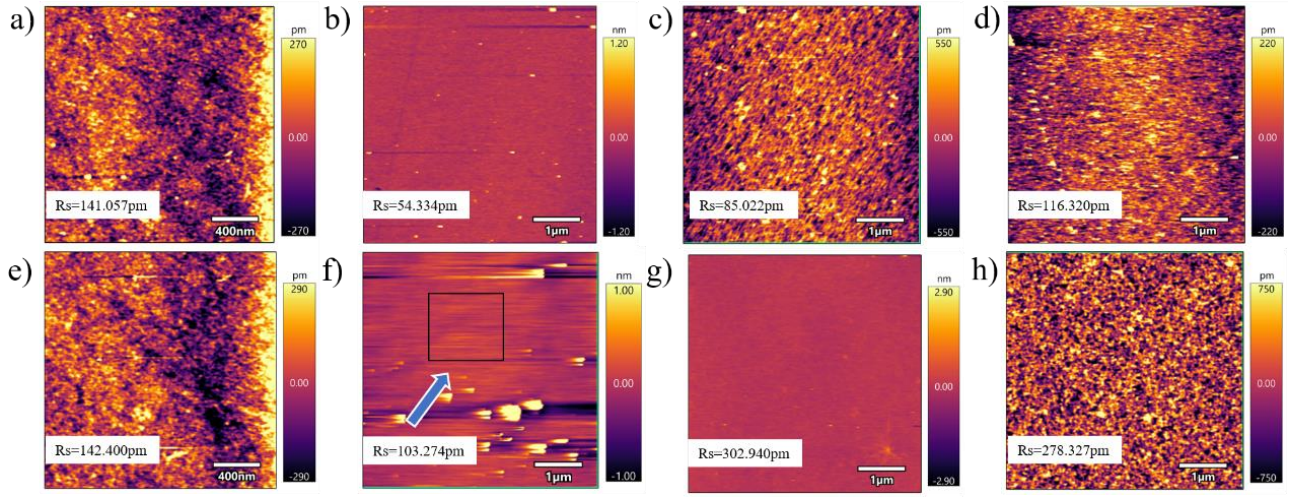

Fig. S7 AFM topography images of silicon electrodes before and after Fc functionalization: **(a)** N(100)-blank; **(b)** P(100)-blank; **(c)** P(110)-blank; **(d)** P(111)-blank; **(e)** N(100)-Fc; **(f)** P(100)-Fc; **(g)** P(110)-Fc; **(h)** P(111)-Fc. The corresponding RMS roughness (R_s) values are indicated on each panel.

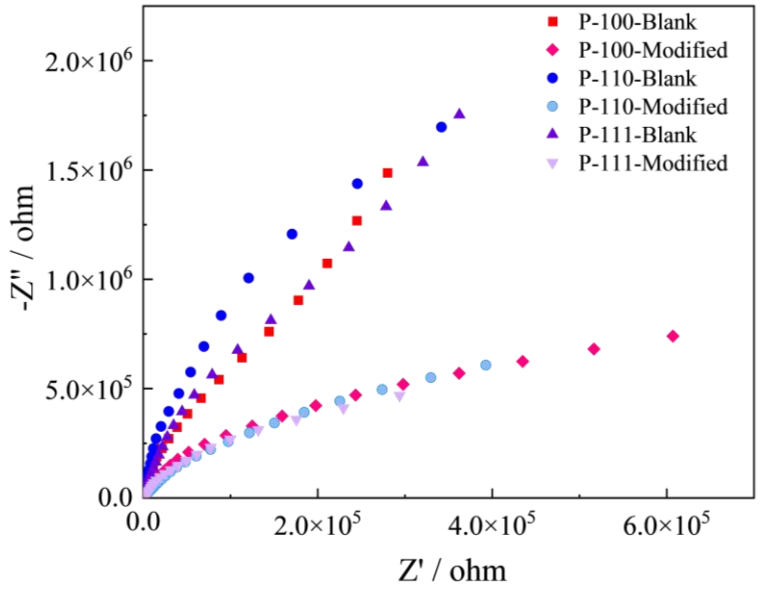

Fig. S8 Nyquist plots of electrochemical impedance spectra (EIS) for p-type Si(100), Si(110), and Si(111) electrodes before (blank) and after Fc functionalization. The spectra show a clear impedance shift upon modification and a distinct facet dependence for the Fc-modified p-type Si electrodes.